



Association of ³⁴S-depleted pyrite layers with negative carbonate $\delta^{13}\text{C}$ excursions at the Permian-Triassic boundary: Evidence for upwelling of sulfidic deep-ocean water masses

Thomas Algeo

Department of Geology, University of Cincinnati, Cincinnati, Ohio 45221-0013, USA (thomas.algeo@uc.edu)

Yanan Shen and Tonggang Zhang

Centre de Recherche en Géochimie et en Géodynamique, Université du Québec à Montréal, C.P. 8888, Succursale Centre-Ville, Montreal, Quebec, Canada H3C 3P8 (shen.yanan@uqam.ca)

Timothy Lyons and Steven Bates

Department of Earth Sciences, University of California, Riverside, California 92521-0423, USA (timothyly@ucr.edu)

Harry Rowe

Department of Geological Sciences, University of Kentucky, Lexington, Kentucky 40506, USA (browe@email.uky.edu)

T. K. T. Nguyen

Institute of Geophysics, Vietnamese Academy of Science and Technology, Hanoi, Vietnam (nkthoa@fpt.vn)

[1] A marine Permian-Triassic boundary (PTB) section at Nhi Tao, Vietnam, contains a series of at least 9 pyritic horizons characterized by concurrent decreases in pyrite S- ($\delta^{34}\text{S}_{\text{py}}$) and carbonate C-isotopic compositions ($\delta^{13}\text{C}_{\text{carb}}$). The first and largest of the events that precipitated these pyritic horizons was coincident with the Late Permian mass extinction, while subsequent events were generally smaller and occurred at quasiperiodic intervals of ~ 20 to 30 ka. A near complete lack of organic carbon to drive bacterial sulfate reduction in sediment pore waters, among other considerations, argues against a diagenetic control for these relationships. Rather, the covariant patterns documented herein are most easily explained as the product of recurrent upwelling of anoxic deep-ocean waters containing ³⁴S-depleted hydrogen sulfide and ¹³C-depleted dissolved inorganic carbon. The sulfide $\delta^{34}\text{S}$ record of the study section represents a mixture of a small amount of isotopically heavy authigenic pyrite (formed via in situ bacterial sulfate reduction) with a generally larger quantity of isotopically light syngenetic pyrite precipitated within the water column during upwelling episodes. Although upwelling of toxic deepwaters has been invoked in earlier studies as a mechanism for the Late Permian marine mass extinction, this is the first study to (1) document patterns of pyrite- $\delta^{13}\text{C}_{\text{carb}}$ covariation that strongly support upwelling as a major process at the PTB and (2) provide evidence of multiple, quasiperiodic upwelling events that may reflect reinvigoration of global-ocean overturn following a prolonged interval of Late Permian deep-ocean stagnation.

Components: 5322 words, 5 figures.

Keywords: P-Tr boundary; S isotopes; carbonate C isotopes; anoxia; extinction.

Index Terms: 4924 Paleooceanography: Geochemical tracers; 4964 Paleooceanography: Upwelling (4279); 4901 Paleooceanography: Abrupt/rapid climate change (1605).

Received 11 September 2007; **Revised** 19 November 2007; **Accepted** 14 December 2007; **Published** 16 April 2008.

Algeo, T., Y. Shen, T. Zhang, T. Lyons, S. Bates, H. Rowe, and T. K. T. Nguyen (2008), Association of ^{34}S -depleted pyrite layers with negative carbonate $\delta^{13}\text{C}$ excursions at the Permian-Triassic boundary: Evidence for upwelling of sulfidic deep-ocean water masses, *Geochem. Geophys. Geosyst.*, 9, Q04025, doi:10.1029/2007GC001823.

1. Introduction

[2] The ~ 252 -million-year-old [Bowring *et al.*, 1998; Mundil *et al.*, 2004] Permian-Triassic boundary (PTB) is associated with the single largest mass extinction event in Earth history, during which $\sim 90\%$ of marine and $\sim 70\%$ of terrestrial taxa disappeared [Erwin, 1994; Retallack, 1995]. The C-isotope chemostratigraphy of the PTB has been the subject of scores of published studies, most of which document a -3 to -8% shift commencing at the Late Permian extinction/event horizon (LPEH), a feature present not only in marine $\delta^{13}\text{C}_{\text{carb}}$ but also in marine and terrestrial $\delta^{13}\text{C}_{\text{org}}$ records [e.g., Baud *et al.*, 1989; Krull and Retallack, 2000; Twitchett *et al.*, 2001; de Wit *et al.*, 2002; Sephton *et al.*, 2002; Krull *et al.*, 2004; Payne *et al.*, 2004; Korte *et al.*, 2004, 2008]. This shift reflects a major perturbation to the global carbon cycle that has been variously attributed to biomass destruction, reduced organic carbon burial, oxidation of methane from seafloor clathrates or coal or of organic matter from soils, and volcanic CO_2 emissions (see Berner [2002] and Erwin *et al.* [2002] for reviews). Because the carbon cycle is subject to so many possible influences, C-isotope data alone do not allow for a unique interpretation of causation.

[3] The existence of deep-ocean anoxia during the Late Permian and Early Triassic is now well established [Wignall and Twitchett, 1996, 2002; Isozaki, 1997; Hotinski *et al.*, 2001; Kiehl and Shields, 2005], and S-isotope studies have provided insights regarding contemporaneous changes in seawater chemistry. Carbonate-associated-sulfate (CAS) $\delta^{34}\text{S}$ records from shallow-marine sections document a rapid negative excursion (-10 to -20%) at the LPEH, followed by a larger positive shift ($+20$ to $+40\%$) during the first ~ 1 Ma of the Early Triassic [Kaiho *et al.*, 2001, 2006; Newton *et al.*, 2004; Riccardi *et al.*, 2006], a pattern of longer-term variation also suggested by pyrite $\delta^{34}\text{S}$ records [Kajiwara *et al.*, 1994; Nielsen and Shen, 2004; Riccardi *et al.*, 2006]. These records have been interpreted to reflect strong bacterial sulfate reduction (BSR) in the Late Permian deep ocean, with upwelling and partial oxidation of

sulfide in shallow-marine environments at the PTB, and subsequent massive burial of pyrite driving seawater sulfate toward more ^{34}S -enriched values during the Early Triassic. These inferences are consistent with independent evidence of transiently anoxic conditions in shallow-marine environments at the PTB based on biomarker and Ce anomaly data [Grice *et al.*, 2005; Xie *et al.*, 2005; Kakuwa and Matsumoto, 2006; Hays *et al.*, 2007; Son *et al.*, 2007].

[4] Paired C- and S-isotopic records have been published for only a few PTB sections to date, and relationships between these records have received only scant attention. The Italian Dolomites section studied by Newton *et al.* [2004] exhibits negative $\delta^{13}\text{C}_{\text{carb}}-\delta^{34}\text{S}_{\text{py}}$ covariation through the Upper Permian but positive covariation within the Lower Triassic (Figure 1), although the rather coarse sample spacing (~ 0.5 to 10 m) within the latter interval makes such inferences tenuous. The Chinese sections at Meishan and Shangsi studied by Riccardi *et al.* [2006, 2007] do not appear to exhibit any C- and S-isotopic covariation, although the possibility of such covariation was not specifically considered. In the present study of the PTB at Nhi Tao, Vietnam, we demonstrate significant positive covariation of pyritic horizons (as proxied by $[\text{S}]_{\text{py}}$ and $\delta^{34}\text{S}_{\text{py}}$) with carbonate $\delta^{13}\text{C}$ at a fine (10 – 20 cm) stratigraphic scale, and we consider the implications of these relationships for understanding causation of the PTB. The Nhi Tao PTB section was examined previously by Algeo *et al.* [2007] and, independently, by Son *et al.* [2007]. In the present contribution, we report results of S-isotopic analyses that were generated subsequent to our earlier paper.

2. Geologic Background

[5] The PTB interval at Nhi Tao, Vietnam, comprises shallow-marine facies of the Jinxi Platform, one of several large (>50 km wide) carbonate platforms within the Nanpanjiang Basin on the southern margin of the south China craton (Figure 2) [Lehrmann *et al.*, 2003; Payne *et al.*, 2004]. During the Late Permian and Early Triassic,

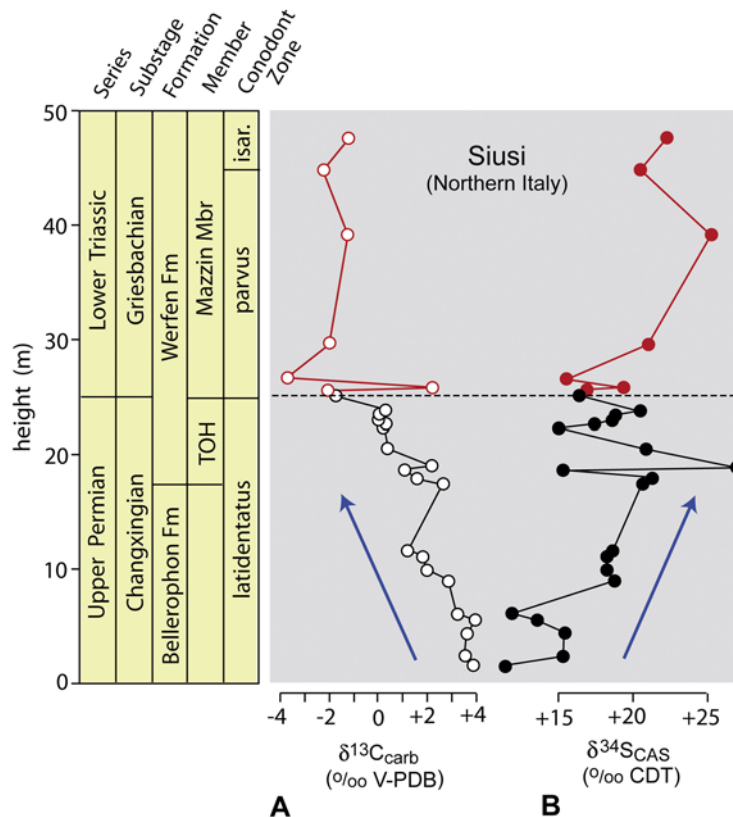


Figure 1. C- and S-isotope stratigraphy of the Siusi PTB section, Italian Dolomites. TOH, Tesero Oolite Horizon. Blue arrows emphasize negative $\delta^{13}\text{C}_{\text{carb}}\text{-}\delta^{34}\text{S}_{\text{py}}$ covariation at a coarse stratigraphic scale through the Upper Permian; red symbols emphasize positive $\delta^{13}\text{C}_{\text{carb}}\text{-}\delta^{34}\text{S}_{\text{py}}$ covariation within the Lower Triassic. Redrawn from *Newton et al.* [2004].

the south China craton was located at tropical latitudes in the eastern half of the Paleotethys Ocean. The study site proved advantageous for an analysis of hydrogenous (seawater-derived) chemostratigraphic signals associated with the PTB owing to its paleogeographic location on an open shelf margin subject to influence by deep water masses and to its relative isolation from terrigenous siliciclastic influx.

[6] The 7.5-m-thick study section ranges from the upper *changxingensis* zone (late Upper Permian) to the lower *isarcica* zone (early Lower Triassic; Figure 3a). The gradualness of stratigraphic variation in $\delta^{13}\text{C}_{\text{carb}}$ and magnetic susceptibility (MS) at Nih Tao suggests that the section does not contain major hiatus and that the PTB interval is stratigraphically complete [Algeo et al., 2007]. The position of the PTB has been constrained on the basis of foraminiferal biostratigraphy and correlation of $\delta^{13}\text{C}_{\text{carb}}$ and MS records with the Global Stratotype Section at Meishan, Zhejiang Province,

China [Algeo et al., 2007; Son et al., 2007]. The Late Permian extinction horizon (LPEH) is located ~ 45 cm below the PTB, at the base of a 12-cm-thick oolitic-pisolitic grainstone event bed. This horizon coincides with an abrupt change in carbonate microfacies, from cherty fossiliferous wackestones-packstones below the LPEH to *Renalcis*-type calcimicrobial framestones above the LPEH. Similar facies patterns are found in carbonate successions throughout the Nanpanjiang Basin [Kershaw et al., 2002; Lehrmann et al., 2003].

3. Methods

[7] C and S concentrations were determined at the U. of Cincinnati using an Eltra 2000 C-S analyzer. Results were calibrated using USGS standards; analytical precision (2σ) was $\pm 2.5\%$ of reported values for C and $\pm 5\%$ for S. An aliquot of each sample was digested in HCl at 50°C for 12 hours, and the residue was analyzed for total organic

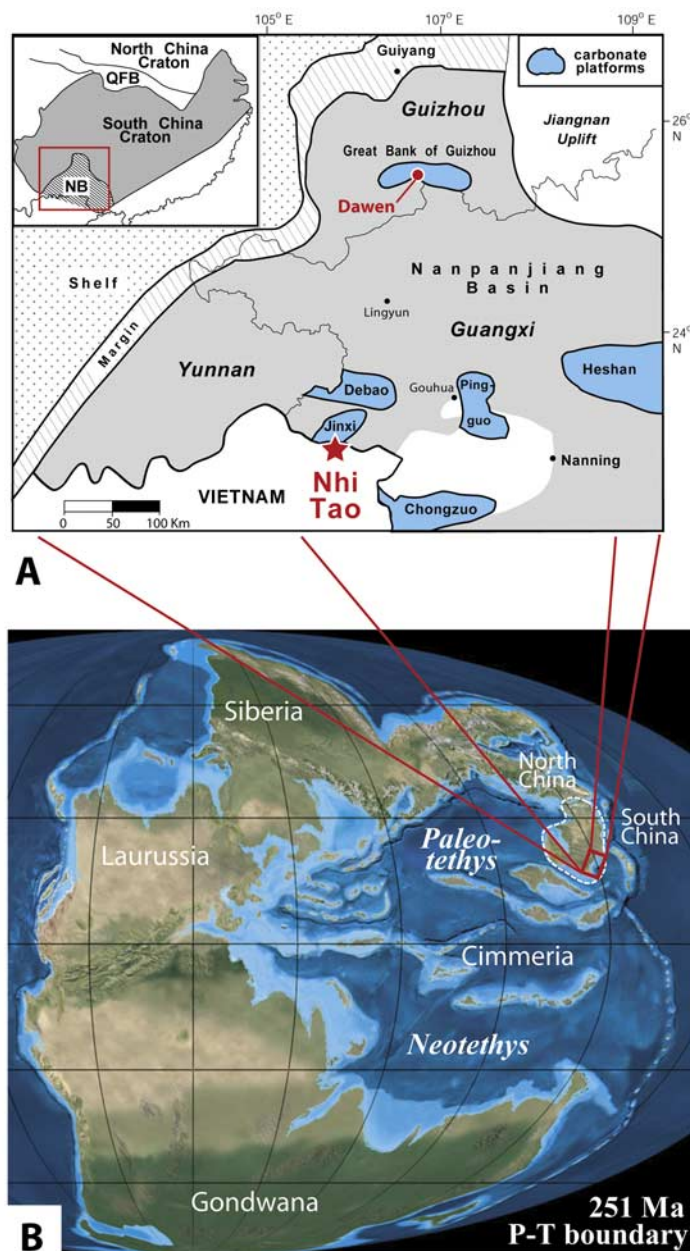


Figure 2. (a) Paleogeography and location map for Nhi Tao. GBG, Great Bank of Guizhou; NB, Nanpanjiang Basin. Modified from *Lehrmann et al.* [2003]. (b) Paleogeography of Tethyan Ocean region at the PTB (251 Ma). ANG, Angara; CM, Cimmeria; GND, Gondwana; NC, North China; PAN, Panthalassic Ocean; SC, south China. Base map courtesy of R. Blakey (<http://jan.ucc.nau.edu/~rcb7/>).

carbon (TOC) and non-acid-volatile sulfur (NAVS). Carbonate $\delta^{13}\text{C}$ - $\delta^{18}\text{O}$ was analyzed at the U. of Kentucky using a GasBench-II peripheral coupled to a DeltaPlusXP isotope-ratio-mass spectrometer. Samples were equilibrated at 40°C for 24 hours before analysis. Analytical precision (2σ) was better than 0.05‰ for both $\delta^{13}\text{C}$ and $\delta^{18}\text{O}$; results are reported relative to the V-PDB standard. S and Fe extractions were performed at the U. of

California at Riverside. Pyrite S was quantitatively extracted by the chromium reduction method of *Canfield et al.* [1986]. The extracted Ag_2S was burned with excess Cu_2O at 1050°C, producing SO_2 gas that was purified on a high-vacuum extraction line and stored in Pyrex break-seal tubes for S-isotopic analysis. S-isotope analyses were performed at both the U. of California at Riverside and the U. of Quebec at Montreal; results have a

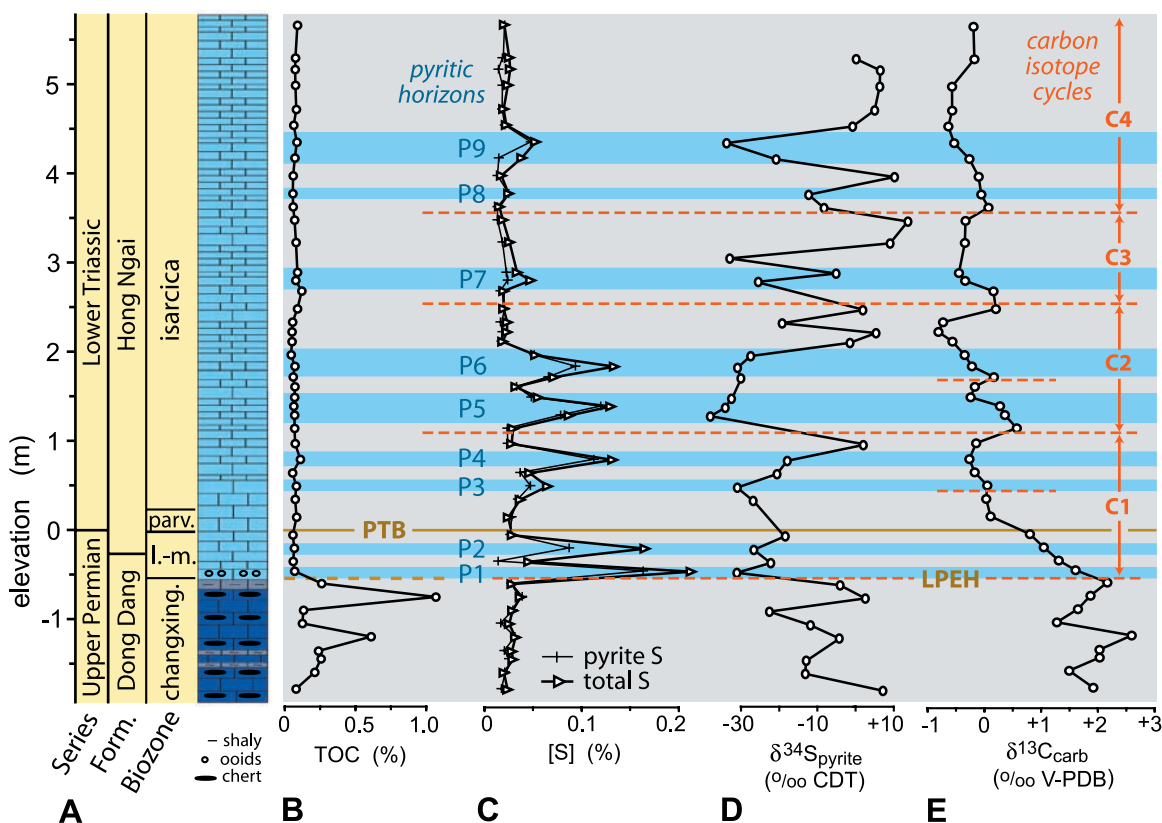


Figure 3. The Nhi Tao section: (a) stratigraphy, (b) TOC, (c) total [S] and pyrite [S], (d) pyrite $\delta^{34}\text{S}$, and (e) carbonate $\delta^{13}\text{C}$. LPEH, Late Permian event horizon; PTB, Permian-Triassic boundary; l.-m., *latidentatus-meishanensis* zone; parv., *parvus* zone; P1–P9, pyritic horizons; C1–C4, carbon isotope cycles.

reproducibility of better than $\pm 0.5\text{‰}$ and are reported relative to the CDT standard.

4. Results

[8] See auxiliary material Tables S1 and S2.¹

[9] The LPEH is associated with major geochemical changes: (1) an abrupt decline in total organic carbon (TOC) to near-zero concentrations (Figure 3b; also seen in other south China PTB sections) [Krull *et al.*, 2004; Riccardi *et al.*, 2006]; (2) the first of 9 pyritic horizons (Figure 3c); (3) the onset of a 5-m-thick interval characterized by locally lower $\delta^{34}\text{S}_{\text{py}}$ values (Figure 3d); and (4) the onset of a sustained -3‰ shift in $\delta^{13}\text{C}_{\text{carb}}$ (Figure 3e). The first pyritic horizon (P1) is the most pyrite rich, and stratigraphically higher horizons exhibit a trend toward lower pyrite S concentrations (Figure 3c). Pyrite $\delta^{34}\text{S}$ values range from -37.8‰ to $+10.0\text{‰}$

CDT with the most ^{34}S -depleted values clustered in a 5-m-thick interval immediately above the LPEH (Figure 3d). The negative $\delta^{13}\text{C}_{\text{carb}}$ shift commencing at the LPEH is initially rapid and reaches a local minimum of $\sim -0.5\text{‰}$ PDB about 1.3 m above the LPEH. Over the next four meters, the $\delta^{13}\text{C}_{\text{carb}}$ record exhibits a series of small-scale ($\sim 1\text{-m}$) fluctuations with amplitudes of $\sim 1\text{‰}$, defining at least four C-isotope cycles (or more, if smaller inflections within cycles C1 and C2 are counted; Figure 3e).

[10] Close examination of the Nhi Tao $[\text{S}]_{\text{py}}$, $\delta^{34}\text{S}_{\text{py}}$, and $\delta^{13}\text{C}_{\text{carb}}$ records reveals significant covariant relationships among them. Each pyritic horizon is associated with a local decrease in $\delta^{34}\text{S}_{\text{py}}$ values ranging from $\sim -5\text{‰}$ to -40‰ in magnitude, whereas pyrite-poor “background” intervals exhibit relatively heavier S-isotopic compositions (Figures 3c and 3d). Negative covariation between $[\text{S}]_{\text{py}}$ and $\delta^{34}\text{S}_{\text{py}}$ is highly statistically significant ($r = -0.74$, $p(\alpha) < 0.001$ for a 2nd-order polynomial fit; Figure 4). Each pyritic horizon is also associated with an interval of decreasing

¹Auxiliary materials are available at <ftp://ftp.agu.org/apend/gc/2007gc001823>.

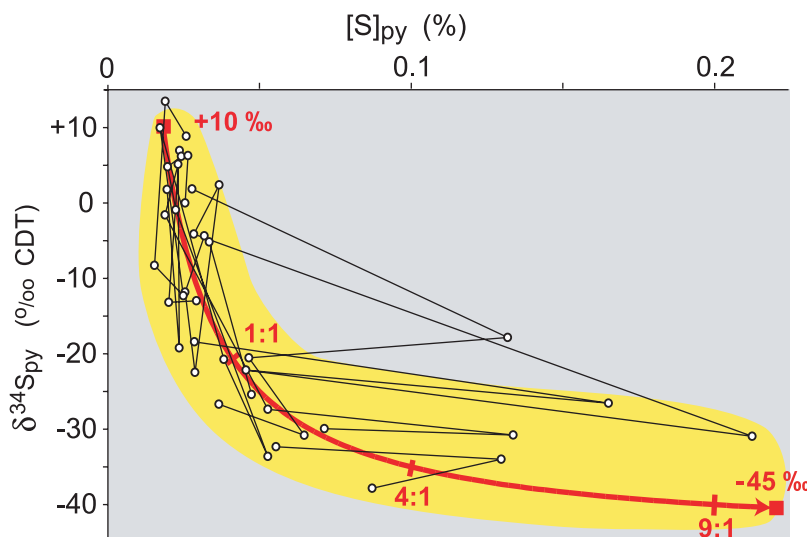


Figure 4. Pyrite $\delta^{34}\text{S}$ versus pyrite $[\text{S}]_{\text{py}}$. Black lines connect stratigraphically adjacent samples. The red curve represents a two-component mixing model with low-S and high-S end-members having $\delta^{34}\text{S} = +10\text{‰}$ and -45‰ and representing authigenic and syngenetic pyrite fractions, respectively; also shown are syngenetic:authigenic pyrite mixing ratios of 1:1, 4:1, and 9:1.

$\delta^{13}\text{C}_{\text{carb}}$ values, with peak pyrite concentrations located mostly at or close to the onset of negative C-isotope excursions (Figures 3c and 3e). This relationship is most obvious for the P1 and P2 horizons, which are associated with the -3‰ $\delta^{13}\text{C}_{\text{carb}}$ shift just above the LPEH, but it exists for all of the other pyritic horizons in the study section as well. P3 and P4 are associated with a negative $\delta^{13}\text{C}_{\text{carb}}$ excursion at the top of cycle C1, P5 and P6 with the onset of negative excursions in cycle C2, P7 with the onset of a negative excursion in cycle C3, and P8 and P9 with the onset and culmination of a negative excursion in cycle C4 (Figure 3e). Covariation between the $\delta^{34}\text{S}_{\text{py}}$ and $\delta^{13}\text{C}_{\text{carb}}$ records is more subtle, but samples with more ^{34}S -enriched values tend to be clustered at the contacts between C-isotopic cycles (i.e., at local $\delta^{13}\text{C}_{\text{carb}}$ maxima), reflecting generally positive covariation at a fine (sub-meter) scale (Figures 3d and 3e).

5. Discussion

[11] A diagenetic explanation for patterns of covariation among $[\text{S}]_{\text{py}}$, $\delta^{34}\text{S}_{\text{py}}$, and $\delta^{13}\text{C}_{\text{carb}}$ is unlikely for several reasons. First, TOC data do not support BSR as the source of sulfide in the Nhi Tao section: no pyritic horizons formed below the LPEH despite TOC values as high as $\sim 1\%$, whereas multiple pyritic horizons are found above the LPEH despite a lack of organic matter ($< 0.1\%$ TOC) to drive bacterial reduction of pore water

sulfate (Figures 3b and 3c). Second, Rayleigh distillation of pore water sulfate would yield positive covariation between $[\text{S}]_{\text{py}}$ and $\delta^{34}\text{S}_{\text{py}}$ [Goldhaber and Kaplan, 1974], inconsistent with the pattern of negative covariation observed in this study (Figure 4). Third, if $[\text{S}]_{\text{py}}-\delta^{13}\text{C}_{\text{carb}}$ covariation were due to oxidation of organic matter and precipitation of diagenetic carbonate within the sediment, then pyritic horizons would correlate with $\delta^{13}\text{C}$ minima (peak organic matter oxidation) and possibly be associated with carbonate nodule layers (due to associated alkalinity increases). In fact, pyritic horizons show a clear association with the onset of negative $\delta^{13}\text{C}_{\text{carb}}$ excursions, and carbonate nodules are absent (Figures 3c and 3e). Fourth, the -3‰ C-isotopic excursion just above the LPEH, which is associated with ^{34}S -depleted pyritic horizons P1 and P2 (Figures 3c and 3e), is known to represent a global environmental signal. If this feature has a (global) environmental origin, then the other, smaller negative C-isotope excursions (C2–C4), which show the same relationships to $[\text{S}]_{\text{py}}$ and $\delta^{34}\text{S}_{\text{py}}$ as C1, can also be inferred to represent responses to an environmental forcing. Finally, if Fe limitation were the primary control on pyrite formation, then $[\text{Fe}]$ would covary positively with $[\text{S}]_{\text{py}}$ and $\delta^{34}\text{S}_{\text{py}}$, and degree-of-pyritization (DOP) values would be high. In fact, $[\text{Fe}]$ exhibits statistically insignificant ($p(\alpha) > 0.05$) relationships with $[\text{S}]_{\text{py}}$ and $\delta^{34}\text{S}_{\text{py}}$, and DOP values above the LPEH are low to intermediate (0.35 ± 0.21). Collectively, these observations favor a primary

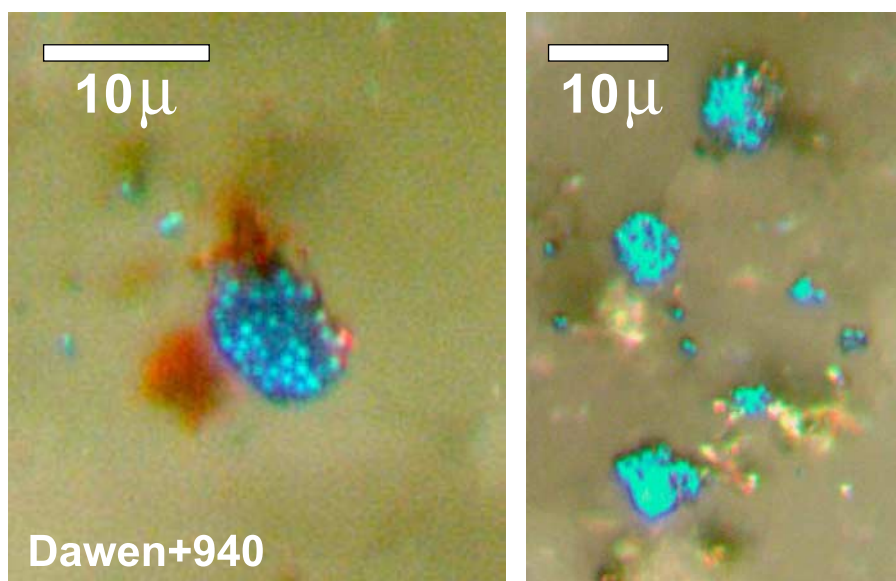


Figure 5. Framboidal pyrite in a sample 940 cm above the PTB at Dawen, Guizhou Province, south China (see Figure 2 for location). The Dawen section is located on the Great Bank of Guizhou, a carbonate platform that accumulated shallow-marine carbonates of similar facies character to those of the Nhi Tao study section [Payne *et al.*, 2007].

(environmental) origin for the chemostratigraphic patterns observed at Nhi Tao.

[12] The relationships discussed above, i.e., the association of pyritic horizons with lower $\delta^{34}\text{S}_{\text{py}}$ and $\delta^{13}\text{C}_{\text{carb}}$ values, limit the range of viable models for the Nhi Tao depositional system. The tight coupling among these proxies implies control by a common environmental process. The most likely mechanisms are upwelling of anoxic deep-ocean water masses [Kajiwara *et al.*, 1994] or chemocline upward excursions [Kump *et al.*, 2005], in either case introducing ^{13}C -depleted dissolved inorganic carbon and ^{34}S -depleted hydrogen sulfide into the ocean surface layer. The nonlinear covariant relationship between $[\text{S}]_{\text{py}}$ and $\delta^{34}\text{S}_{\text{py}}$ was probably the product of a two-component mixing system, in which a relatively fixed quantity ($\sim 0.02\%$) of authigenic pyrite having a ^{34}S -enriched composition (~ 0 to $+10\%$; derived via near-quantitative BSR of Late Permian seawater sulfate [Strauss, 1997]) was diluted by variable amounts of ^{34}S -depleted ($\sim -45\%$) syngenetic pyrite formed during upwelling events (Figure 4). The strongly ^{34}S -depleted composition of the latter end-member was due to the generation of H_2S under open-system (non-sulfate-limited) conditions in the anoxic Late Permian deep ocean [Wignall and Twitchett, 1996, 2002; Isozaki, 1997]. Although Nhi Tao samples were too small to allow petrographic analysis, study of thin sections

from another PTB section in the Nanpanjiang Basin (Dawen; Figure 5) has revealed numerous clusters of small ($\sim 3\text{--}6\ \mu$) pyrite framboids of probable syngenetic origin distributed throughout the sample matrix [cf. Wilkin *et al.*, 1996; Wignall and Newton, 1998; Nielsen and Shen, 2004; Wignall *et al.*, 2005].

[13] Although upwelling of sulfidic deep-ocean waters has been proposed in earlier studies [Kajiwara *et al.*, 1994; Knoll *et al.*, 1996; Wignall and Twitchett, 1996, 2002; Isozaki, 1997], the present study provides important new insights in demonstrating the occurrence of multiple episodes of upwelling along the margin of the south China craton at quasiperiodic intervals of $\sim 20\text{--}30$ ka. Peri-equatorial upwelling in the eastern Paleotethys is consistent with Permian oceanic modeling results [Kutzbach *et al.*, 1990; Winguth *et al.*, 2002]. Algeo *et al.* [2007] hypothesized that these episodes occurred in response to reinvigoration of oceanic overturn following a prolonged interval of Late Permian deep-ocean stagnation. Stagnation of the Late Permian ocean did not require complete cessation of deepwater formation but, rather, only a reduction in the rate of vertical overturn and deepwater ventilation. Circulation in the modern ocean is thought to oscillate between several “modes” owing to changes in atmospheric water vapor transport, freshwater influx, and other factors, with resultant variation in rates of oceanic



ventilation at both millennial and longer timescales [Broecker and Denton, 1989; Burton et al., 1997; Hillaire-Marcel et al., 2001; Elliot et al., 2002]. With regard to Permian-Triassic oceans, modeling studies have implicated flatter latitudinal temperature gradients, increased freshwater discharge, higher nutrient inventories, and enhanced particle ballasting as possible factors contributing to deep-ocean anoxia [Hotinski et al., 2001; Kiehl and Shields, 2005; Winguth and Maier-Reimer, 2005]. Also possible is a switch between high-latitude cold and low-latitude warm-saline deepwater formation [Wilde and Berry, 1982], as the warmer bottomwater temperatures associated with the latter mode would result in significantly lower dissolved oxygen concentrations [Hotinski et al., 2001].

[14] An alternative to the oceanic-overturn model of Algeo et al. [2007] is the chemocline-upward-excursion model proposed by Kump et al. [2005] and tested by Riccardi et al. [2006, 2007]. Although both models assume the existence of a shallow oceanic chemocline as a starting point, a key difference is the nature of the climatic trigger causing transfer of deep-ocean hydrogen sulfide to shallow-marine systems. Whereas the trigger in the oceanic-overturn model is abrupt climatic cooling due to onset of Siberian Trap volcanism [Renne et al., 1995; Korte et al., 2008], the chemocline-upward-excursion model assumes that warming and oceanic stagnation intensify until the chemocline shallows to the point of instability, causing hydrogen sulfide to erupt into the atmosphere and thence to enter surface waters. This issue cannot be resolved at present, but because these two models make diametrically opposed predictions regarding climatic forcing of sulfide-flux events, they may be testable if a suitable proxy (e.g., conodont $\delta^{18}\text{O}$) can be measured at the necessary level of stratigraphic resolution. Existing conodont $\delta^{18}\text{O}$ [Korte et al., 2004, 2008] document a $\sim 4\text{--}6^\circ\text{C}$ warming from the Late Permian into the Early Triassic, but the level of stratigraphic resolution is much too coarse to evaluate the relationship of climate change to high-frequency sulfide-flux events.

6. Conclusions

[15] The PTB section at Nhi Tao, Vietnam, contains at least 9 pyritic horizons of probable syngenetic origin characterized by strongly ^{34}S -depleted sulfur isotopic compositions. A consistent stratigraphic relationship of these horizons to the onset of negative carbonate $\delta^{13}\text{C}$ excursions is most easily explained as the product of recurrent up-

welling of anoxic deep-ocean waters that contained ^{34}S -depleted hydrogen sulfide and ^{13}C -depleted dissolved inorganic carbon. The pyritic horizons commence at the Late Permian extinction horizon and are found at quasi-regular intervals over the next ~ 5 meters of section, suggesting that upwelling occurred along the southern margin of the south China craton with a periodicity of $\sim 20\text{--}30$ ka, i.e., consistent with control by climate variation at orbital timescales. The broader significance of this pattern may be as a record of reinvigorated global-ocean overturn following a prolonged interval of stagnation during the Late Permian, during which the oceanic chemocline rose to relatively shallow depths. This is the first published study to document a strong relationship between pyrite horizons and carbonate $\delta^{13}\text{C}$ trends at the Permian-Triassic boundary. The evidence from Nhi Tao offers no support for an extraterrestrial cause for the PTB [cf. Becker et al., 2001].

Acknowledgments

[16] We thank Barry Maynard and Bob King for analytical assistance and Jesper Kresten Nielsen, Lee Kump, and Laurent Labeyrie for constructive reviews of the manuscript. This project was supported in part by grants to T.J.A. from the National Science Foundation (EAR-0310072 and EAR-0618003) and the University of Cincinnati Research Council.

References

- Algeo, T. J., B. B. Ellwood, T. K. T. Nguyen, H. Rowe, and J. B. Maynard (2007), The Permian-Triassic boundary at Nhi Tao, Vietnam: Evidence for recurrent influx of sulfidic watermasses to a shallow-marine carbonate platform, *Palaeogeogr. Palaeoclimatol. Palaeoecol.*, 252, 304–327, doi:10.1016/j.palaeo.2006.11.055.
- Baud, A., W. T. Holser, and M. Magaritz (1989), Permian-Triassic of the Tethys: Carbon isotope studies, *Geol. Rundsch.*, 78, 649–677.
- Becker, L., R. J. Poreda, A. G. Hunt, T. E. Bunch, and M. Rampino (2001), Impact event at the Permian-Triassic boundary: Evidence from extraterrestrial noble gases in fullerenes, *Science*, 291, 1530–1533.
- Berner, R. A. (2002), Examination of hypotheses for the Permian-Triassic boundary extinction by carbon cycle modeling, *Proc. Natl. Acad. Sci. U.S.A.*, 99, 4172–4177.
- Bowring, S. A., D. H. Erwin, Y. G. Jin, M. W. Martin, K. Davidek, and W. Wang (1998), U/Pb zircon geochronology and tempo of the end-Permian mass extinction, *Science*, 280, 1039–1045.
- Broecker, W. S., and G. H. Denton (1989), The role of ocean-atmosphere reorganizations in glacial cycles, *Geochim. Cosmochim. Acta*, 53, 2465–2501.
- Burton, K. W., H.-F. Ling, and R.-K. O’Nions (1997), Closure of the Central American Isthmus and its effect on deep-water formation in the North Atlantic, *Nature*, 386, 382–385.
- Canfield, D. E., R. Raiswell, J. T. Westrich, C. M. Reaves, and R. A. Berner (1986), The use of chromium reduction in the



- analysis of reduced inorganic sulfur in sediments and shales, *Chem. Geol.*, *54*, 149–155.
- de Wit, M. J., J. G. Ghosh, S. de Villiers, N. Rakotosolofo, J. Alexander, A. Tripathi, and C. Looy (2002), Multiple organic carbon isotope reversals across the Permo-Triassic boundary of terrestrial Gondwana sequences: Clues to extinction patterns and delayed ecosystem recovery, *J. Geol.*, *110*, 227–240.
- Elliot, M., L. Labeyrie, and J. C. Duplessy (2002), Changes in North Atlantic deep-water formation associated with the Dansgaard-Oeschger temperature oscillations (60–10 ka), *Quat. Sci. Rev.*, *21*, 1153–1165.
- Erwin, D. H. (1994), The Permo-Triassic extinction, *Nature*, *367*, 231–236.
- Erwin, D. H., S. A. Bowring, Y.-G. Jin (2002), End-Permian mass-extinctions: A review, in *Catastrophic Events and Mass Extinctions: Impacts and Beyond*, edited by C. Koeberl and K. G. MacLeod, *Spec. Pap. Geol. Soc. Am.*, *356*, 353–383.
- Goldhaber, M. B., and I. R. Kaplan (1974), The sulfur cycle, in *The Sea*, vol. 5, *Marine Chemistry*, edited by E. D. Goldberg, pp. 569–655, John Wiley, New York.
- Grice, K., C. Cao, G. D. Love, M. E. Böttcher, R. J. Twitchett, E. Grosjean, R. E. Summons, S. C. Turgeon, W. Dunning, and Y. Jin (2005), Photic zone euxinia during the Permian-Triassic superanoxic event, *Science*, *307*, 706–709.
- Hays, L. E., T. Beatty, C. M. Henderson, G. D. Love, and R. E. Summons (2007), Evidence for photic zone euxinia through the end-Permian mass extinction in the Panthalassic Ocean (Peace River Basin, Western Canada), *Palaeoworld*, *16*, 39–50.
- Hillaire-Marcel, C., A. de Vernal, G. Bilodeau, and A. J. Weaver (2001), Absence of deep-water formation in the Labrador Sea during the last interglacial period, *Nature*, *410*, 1073–1077.
- Hotinski, R. M., K. L. Bice, L. R. Kump, R. G. Najjar, and M. A. Arthur (2001), Ocean stagnation and end-Permian anoxia, *Geology*, *29*, 7–10.
- Isozaki, Y. (1997), Permo-Triassic boundary superanoxia and stratified superocean: Records from lost deep sea, *Science*, *276*, 235–238.
- Kaiho, K., T. Kajiwara, T. Nakano, Y. Muira, H. Kawahata, K. Tazaki, M. Ueshima, Z. Chen, and G. R. Shi (2001), End-Permian catastrophe by a bolide impact: Evidence of a gigantic release of sulfur from the mantle, *Geology*, *29*, 815–818.
- Kaiho, K., Z.-Q. Chen, H. Kawahata, Y. Kajiwara, and H. Sato (2006), Close-up of the end-Permian mass extinction horizon recorded in the Meishan section, south China: Sedimentary, elemental, and biotic characterization and a negative shift of sulfate sulfur isotope ratio, *Palaeogeogr. Palaeoclimatol. Palaeoecol.*, *239*, 396–405.
- Kajiwara, Y., S. Yamakita, K. Ishida, H. Ishiga, and A. Imai (1994), Development of a largely anoxic stratified ocean and its temporary massive mixing at the Permian-Triassic boundary supported by the sulfur isotope record, *Palaeogeogr. Palaeoclimatol. Palaeoecol.*, *111*, 367–379.
- Kakuwa, Y., and R. Matsumoto (2006), Cerium negative anomaly just before the Permian and Triassic boundary event: The upward expansion of anoxia in the water column, *Palaeogeogr. Palaeoclimatol. Palaeoecol.*, *229*, 335–344.
- Kershaw, S., L. Guo, A. Swift, and J.-S. Fan (2002), Microbialites in the Permian-Triassic boundary interval in central China: Structure, age and distribution, *Facies*, *47*, 83–90.
- Kiehl, J. T., and C. A. Shields (2005), Climate simulation of the latest Permian: Implications for mass extinction, *Geology*, *33*, 757–760.
- Knoll, A. H., R. K. Bambach, D. E. Canfield, and J. P. Grotzinger (1996), Comparative Earth history and Late Permian mass extinction, *Science*, *273*, 452–457.
- Korte, C., H. W. Kozur, M. M. Joachimski, H. Strauss, J. Veizer, and L. Schwark (2004), Carbon, sulfur, oxygen and strontium isotope records, organic geochemistry and biostratigraphy across the Permian/Triassic boundary in Abadeh, Iran, *Int. J. Earth Sci.*, *93*, 565–581.
- Korte, C., P. Pande, P. Kalia, H. W. Kozur, M. M. Joachimski, and H. Oberhänsli (2008), Massive volcanism at the Permian-Triassic boundary and its impact on the isotopic composition of the ocean and atmosphere, *J. Asian Earth Sci.*, in press.
- Krull, E. S., and G. J. Retallack (2000), $\delta^{13}\text{C}_{\text{org}}$ depth profiles from paleosols across the Permian-Triassic boundary: Evidence for methane release, *Geol. Soc. Am. Bull.*, *112*, 1459–1472.
- Krull, E. S., D. J. Lehrmann, D. Druke, B. Kessel, Y. Yu, and R. Li (2004), Stable carbon isotope stratigraphy across the Permian-Triassic boundary in shallow marine carbonate platforms, Nanpanjiang Basin, south China, *Palaeogeogr. Palaeoclimatol. Palaeoecol.*, *204*, 297–315.
- Kump, L. R., A. Pavlov, and M. A. Arthur (2005), Massive release of hydrogen sulfide to the surface ocean and atmosphere during intervals of oceanic anoxia, *Geology*, *33*, 397–400.
- Kutzbach, J. E., P. J. Guetter, and W. M. Washington (1990), Simulated circulation of an idealized ocean for Pangaean time, *Paleoceanography*, *5*, 299–317.
- Lehrmann, D. J., J. L. Payne, S. V. Felix, P. M. Dillett, H. Wang, Y. Yu, and J. Wei (2003), Permian-Triassic boundary sections from shallow-marine carbonate platforms of the Nanpanjiang Basin, south China: Implications for oceanic conditions associated with the end-Permian extinction and its aftermath, *Palaaios*, *18*, 138–152.
- Mundil, R., K. R. Ludwig, I. Metcalfe, and P. R. Renne (2004), Age and timing of the Permian mass extinctions: U/Pb dating of closed-system zircons, *Science*, *305*, 1760–1763.
- Newton, R. J., E. L. Peivitt, P. B. Wignall, and S. H. Bottrell (2004), Large shifts in the isotopic composition of seawater sulphate across the Permo-Triassic boundary in northern Italy, *Earth Planet. Sci. Lett.*, *218*, 331–345.
- Nielsen, J. K., and Y. Shen (2004), Evidence for sulfidic deep water during the Late Permian in the East Greenland Basin, *Geology*, *32*, 1037–1040.
- Payne, J. L., D. J. Lehrmann, J. Wei, M. J. Orchard, D. P. Schrag, and A. H. Knoll (2004), Large perturbations of the carbon cycle during recovery from the end-Permian extinction, *Science*, *305*, 506–509.
- Payne, J. L., D. J. Lehrmann, D. Follett, M. Seibel, L. R. Kump, A. Riccardi, D. Altiner, H. Sano, and J. Wei (2007), Erosional truncation of uppermost Permian shallow-marine carbonates and implications for Permian-Triassic boundary events, *Geol. Soc. Am. Bull.*, *119*, 771–784.
- Renne, P. R., Z. C. Zheng, M. A. Richards, M. T. Black, and A. R. Basu (1995), Synchrony and causal relations between Permian-Triassic boundary crisis and Siberian flood volcanism, *Science*, *269*, 1413–1416.
- Retallack, G. J. (1995), Permian-Triassic extinction on land, *Science*, *267*, 77–80.
- Riccardi, A. L., M. A. Arthur, and L. R. Kump (2006), Sulfur isotopic evidence for chemocline upward excursions during the end-Permian mass extinction, *Geochim. Cosmochim. Acta*, *70*, 5740–5752.
- Riccardi, A., L. R. Kump, M. A. Arthur, and S. D'Hondt (2007), Carbon isotopic evidence for chemocline upward



- excursions during the end-Permian event, *Palaeogeogr. Palaeoclimatol. Palaeoecol.*, **248**, 73–81.
- Sephton, M. A., H. Brinkhuis, C. V. Looy, R. J. Veefkind, H. Visscher, and J. W. de Leeuw (2002), Synchronous record of $\delta^{13}\text{C}$ shifts in the oceans and atmosphere at the end of the Permian, in *Catastrophic Events and Mass Extinctions: Impacts and Beyond*, edited by C. Koeberl and K. G. MacLeod, *Spec. Pap., Geol. Soc. Am.*, **356**, 455–462.
- Son, T. H., C. Koeberl, N. L. Ngoc, and D. T. Huyen (2007), The Permian-Triassic boundary sections in northern Vietnam (Nhi Tao and Lung Cam sections): Carbon-isotope excursion and elemental variations indicate major anoxic event, *Palaeoworld*, **16**, 51–66.
- Strauss, H. (1997), The isotopic composition of sedimentary sulfur through time, *Paleogeogr. Palaeoclimatol. Paleocool.*, **132**, 97–118.
- Twitchett, R. J., C. V. Looy, R. Morante, H. Visscher, and P. B. Wignall (2001), Rapid and synchronous collapse of marine and terrestrial ecosystems during the end-Permian biotic crisis, *Geology*, **29**, 351–354.
- Wignall, P. B., and R. Newton (1998), Pyrite framboid diameter as a measure of oxygen deficiency in ancient mudrocks, *Am. J. Sci.*, **298**, 537–552.
- Wignall, P. B., and R. J. Twitchett (1996), Oceanic anoxia and the end Permian mass extinction, *Science*, **272**, 1155–1158.
- Wignall, P. B., R. J. Twitchett, (2002), Extent, duration and nature of the Permian-Triassic superanoxic event, in *Catastrophic Events and Mass Extinctions: Impacts and Beyond*, edited by C. Koeberl and K. G. MacLeod, *Spec. Pap. Geol. Soc. Am.* **356**, 395–413.
- Wignall, P. B., R. Newton, and M. E. Brookfield (2005), Pyrite framboid evidence for oxygen-poor deposition during the Permian-Triassic crisis in Kashmir, *Palaeogeogr. Palaeoclimatol. Palaeoecol.*, **216**, 183–188.
- Wilde, P., W. B. N. Berry (1982), Progressive ventilation of the oceans—Potential for return to anoxic conditions in the post-Paleozoic, in *Nature and Origin of Cretaceous Carbon-Rich Facies*, edited by S. O. Schlanger and M. B. Cita, pp. 209–224, Academic, New York.
- Wilkin, R. T., H. L. Barnes, and S. L. Brantley (1996), The size distribution of framboidal pyrite in modern sediments: An indicator of redox conditions, *Geochem. Cosmochim. Acta*, **60**, 3897–3912.
- Winguth, A. M. E., and E. Maier-Reimer (2005), Causes of marine productivity and oxygen changes associated with the Permian-Triassic boundary: A reevaluation with ocean general circulation models, *Mar. Geol.*, **217**, 283–304.
- Winguth, A. M. E., C. Heinze, J. E. Kutzbach, E. Maier-Reimer, U. Mikolajewicz, D. Rowley, A. Rees, and A. M. Ziegler (2002), Simulated warm polar currents during the middle Permian, *Paleoceanography*, **17**(4), 1057, doi:10.1029/2001PA000646.
- Xie, S., R. D. Pancost, H. Yin, H. Wang, and R. P. Evershed (2005), Two episodes of microbial change coupled with Permian-Triassic faunal mass extinction, *Nature*, **434**, 494–497.